Supporting information

Light-modulated liquid crystal elastomer-based actuator with multimodal shape morphing and multifunction

Tonghui Zhao[a,b,c], Yanlin Zhang [b,c], Yangyang Fan [b,c], Jiao Wang[a,b,c], Hanqing Jiang [b,c], Jiu-an Lv*[b,c]

[a]School of Materials Science and Engineering, Zhejiang University, Hangzhou 310027, China.

[b]Key Laboratory of 3D Micro/Nano Fabrication and Characterization of Zhejiang Province, School of Engineering, Westlake University, 18 Shilongshan Road, Hangzhou 310024, Zhejiang Province, China.

[c]Institute of Advanced Technology, Westlake Institute for Advanced Study, 18 Shilongshan Road, Hangzhou 310024, Zhejiang Province, China.

*Corresponding author

Email: lvjiuan@westlake.edu.cn

1. Synthesis of NIR-monomer
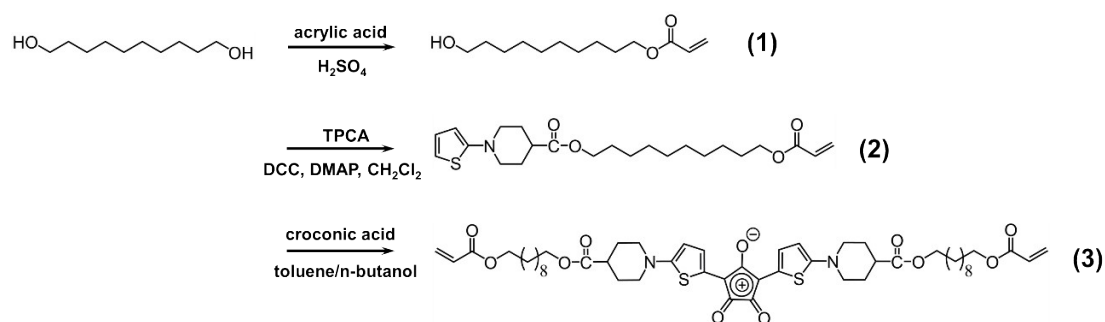

Figure S1. Synthesis route for NIR-monomer

10-hydroxydecyl acrylate (1). A mixture of 1,10-ddecanediol (15g, 86.07 mmol), ten drops of sulfuric acid and inhibitor 4-methoxyphenol (0.5g, 4.03 mmol) were added into a 250 ml three-neck round-bottom flask. The mixture was heated and magnetically stirred at 110 °C under nitrogen atmosphere until the mixture completely melted. Acrylic acid (6.19g, 86.07 mmol) was dropwise added into above mixture for 1h. After reaction for another 5h, the mixture was cooling to room temperature and was washed with brine, dried over $MgSO_4$. The crude product was further purified by column chromatography (ethyl acetate/n-hexane: 10/90) to give compound **1** as yellowish clear liquid (10.41g, yield 53.06%). ^{1}H NMR (500MHz, $CDCl_3$, δ):6.38 (m, 1H), 6.12 (m, 1H), 5.82 (m, 1H), 4.15 (m, 2H), 3.64 (m, 2H), 1.67 (m, 2H), 1.57 (m, 2H), 1.30 (m, 12H).

10-(acryloyloxy)decyl 1-(thiophen-2-yl)piperidine-4-carboxylate (2). In a 500 mL three-neck round-bottom flask, a mixture of compound 1 (2.16 g, 9.47 mmol), 1-thiophen-2-yl-piperidine-4-carboxylic acid (**TPCA**) (2.00 g, 9.47 mmol), DMAP (0.2 g, 1.64 mmol) and DCC (2 g, 9.70 mmol) were suspended in 50 mL of anhydrous dichloromethane under a nitrogen atmosphere. **TPCA** was synthesized according to

previously reported method.[1] The mixture was stirred at room temperature for 24 h. The resulting suspension was filtered to remove the solid residue, and the filtrate was collected and concentrated by rotary evaporation. The raw product was further purified by column chromatography (ethyl acetate/n-hexane: 10/90) to give compound **2** as a yellowish clear liquid (1.45 g, yield 36.4 %). ^{1}H NMR (500 MHz, CDCl$_3$) δ: 6.75 (m, 1H), 6.60 (m, 1H), 6.38 (m, 1H), 6.13 (m, 2H), 5.82 (m, 1H), 4.15 (m, 4H), 4.09 (m, 4H), 3.49 (m, 2H), 2.83 (m, 2H), 2.42 (m, 1H), 2.00 (m, 2H), 1.91 (m, 2H), 1.64 (m, 4H), 1.30 (m, 12H). ^{13}C NMR (500 MHz, CDCl$_3$) δ: 166.42, 130.48, 128.64, 116.01, 114.80, 64.73, 63.07, 55.78, 32.77, 29.48, 29.41, 29.37, 29.21, 28.60, 25.90, 25.71.

Two-acrylic ester-tailed thiophene-croconaine (NIR-monomer) (3). In 250 mL three-neck round-bottom flask, compound **2** (1.22 g, 2.90 mmol), croconic acid (205.80 mg, 1.44 mmol) were dissolved in 100 mL solution of toluene/n-butanol (v/v, 1/1) under nitrogen atmosphere. The mixture was refluxed at 90°C for 2 h. The solvent was evaporated, and the crude product was purified by column chromatography (ethyl acetate and methanol) to provide the final black product (1.02 g, yield 71.53 %). ^{1}H NMR (500 MHz, CDCl$_3$) δ: 8.71 (m, 2H), 6.56 (m, 2H), 6.37 (m, 2H), 6.12 (m, 2H), 5.82 (m, 2H), 4.15 (m, 8H), 3.98 (m, 4H), 3.46 (m, 4H), 2.67 (m, 2H), 2.11 (m, 4H), 1.95 (m, 4H), 1.67 (m, 8H), 1.31 (m, 24H). ^{13}C NMR (500 MHz, CDCl$_3$) δ: 173.36, 166.37, 130.49, 128.64, 65.21, 64.68, 29.78, 29.41, 29.19, 28.60, 28.58, 25.89. ESI-MS m/z: 950.4474 [m + H]$^+$, calculated for compound **3**: 949.2212.
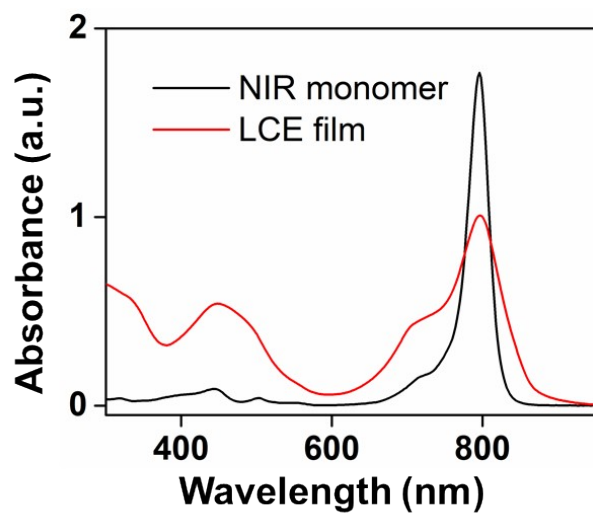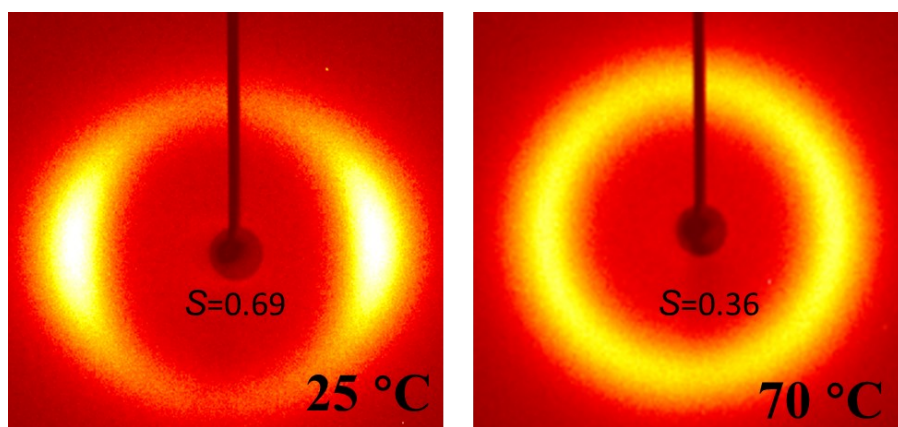
2. Supplementary Figures
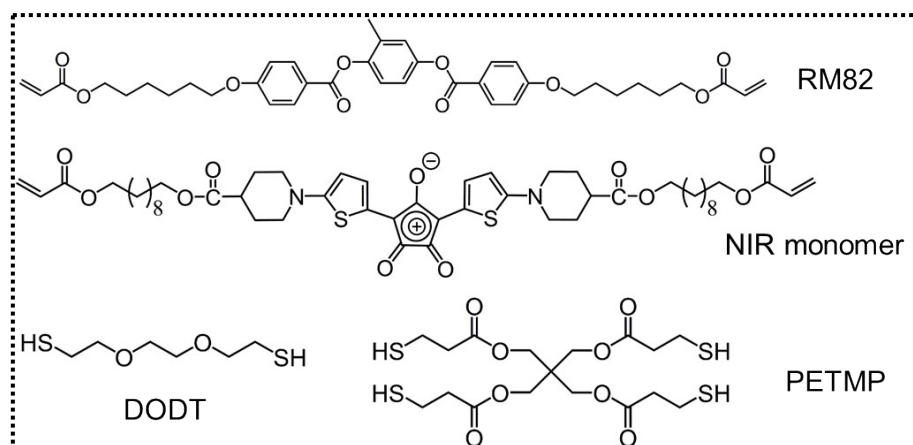
Figure S2. Chemical compositions of LCE material described to prepare millirobots.
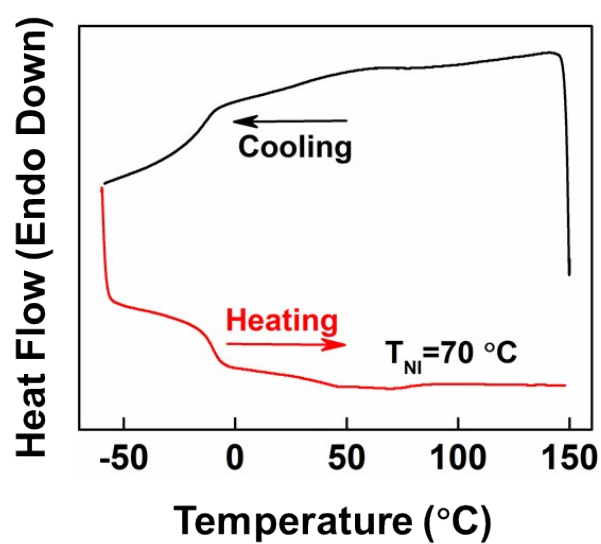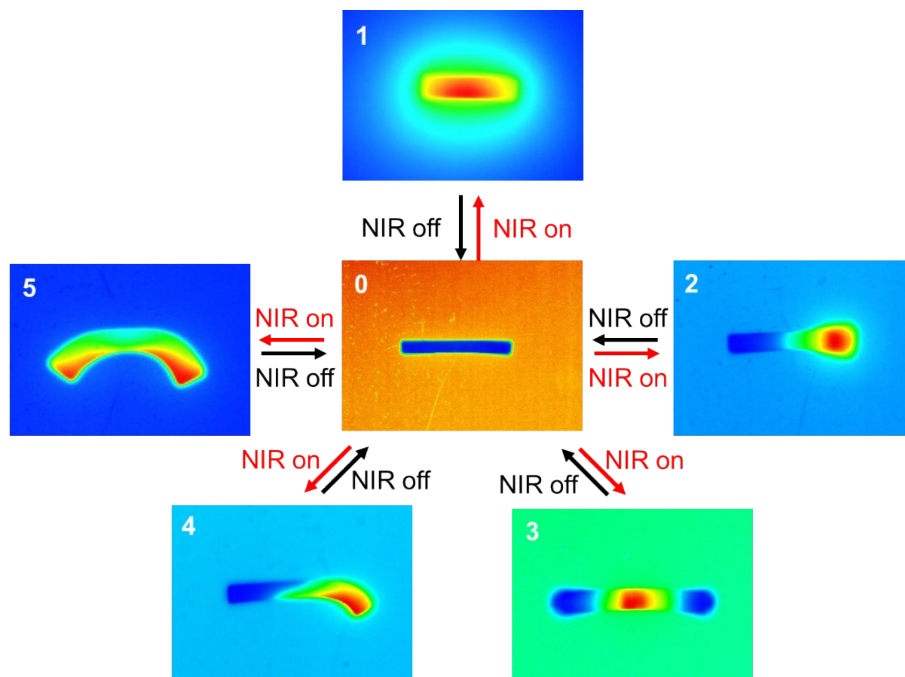

Figure S3. DSC curves about second heating and first cooling stage of millirobot.

Figure S4. The UV-Vis-NIR absorption spectra of NIR monomer in dichloromethane solution and LCE film.

Figure S5. The 2D WAXD patterns of the millirobot at 25 °C and 70 °C. The order parameter (S) of millirobot are 0.69 and 0.36 at 25°C and 70 °C, respectively.

Figure S6. Top view of thermal imaging of five shape morphing 3D structure induced by NIR light in different directions and locations.
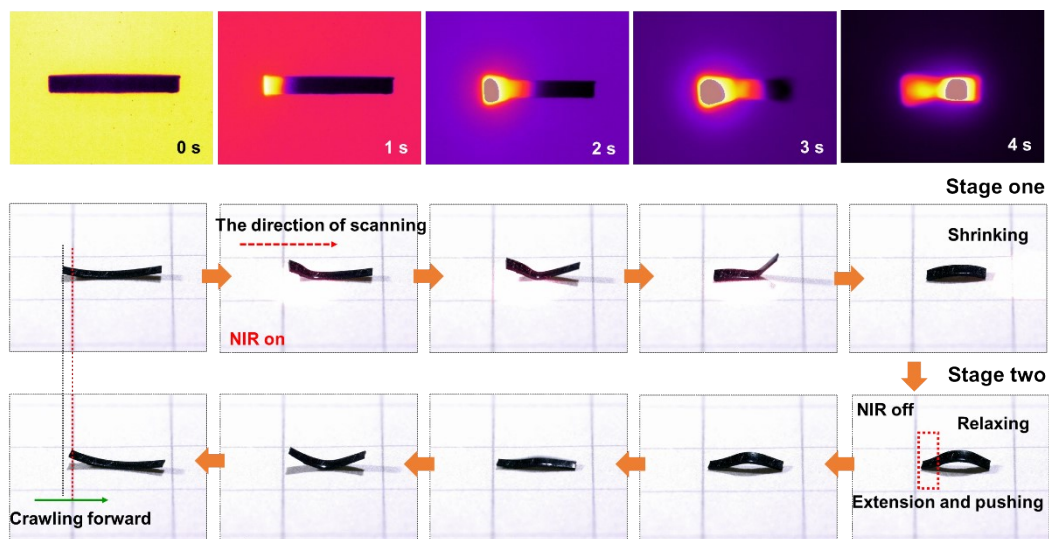

Figure S7. The crawling gait of millirobot. The gait divides two stages including shrinking stage and relaxing stage. The crawling direction is consistent with the scanning direction of NIR spot. Thermal imaging demonstrates the temperature profile

and scanning strategy.
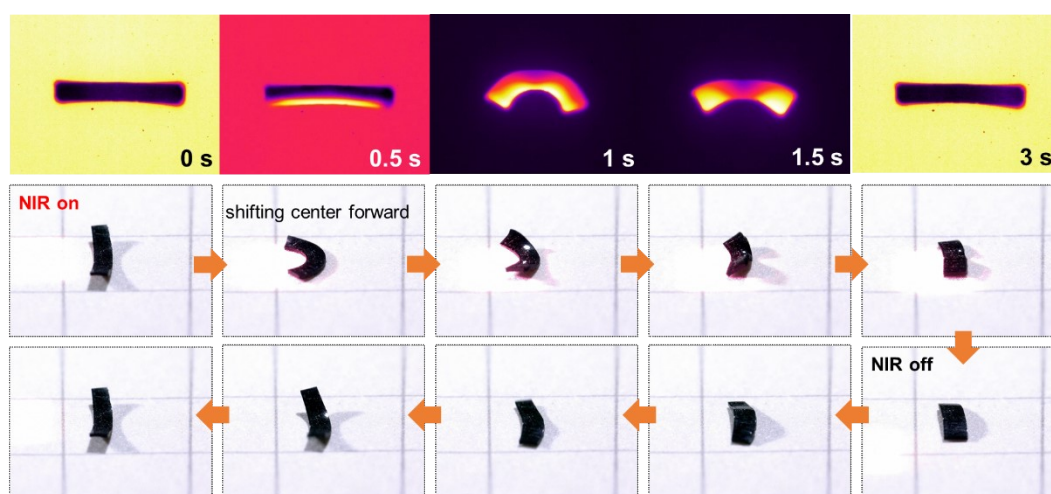
Figure S8. The shifting gait of millirobot. Thermal imaging indicates the stimulated strategy to control millirobot shifting upon switching on/off NIR light.
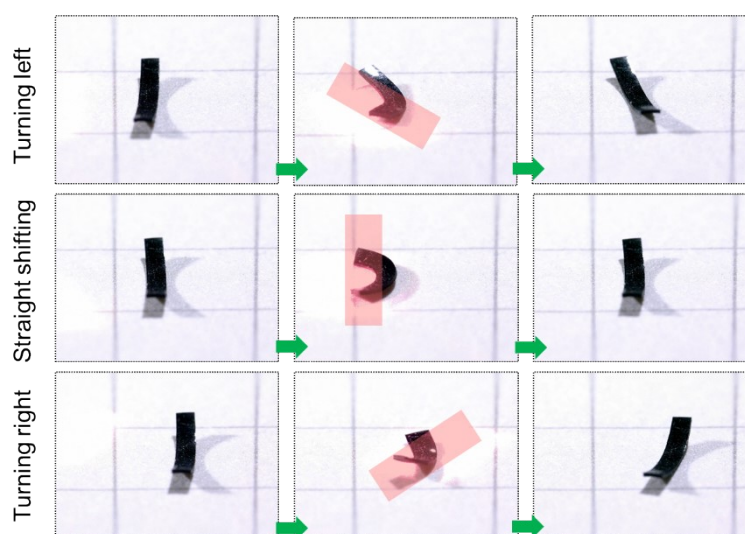
Figure S9. The direction turning of shifting for millirobot. Changing the incident angle of NIR spot provides symmetric/asymmetric morphing of millirobot to tailor the shifting directions.
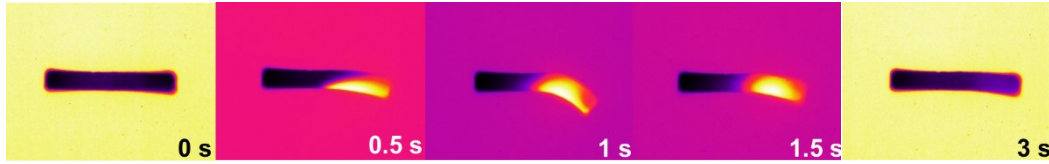
Figure S10. Thermal imaging about Morphing Mode 4 presents the temperature profile induced by corresponding irradiated location and direction about NIR spot.
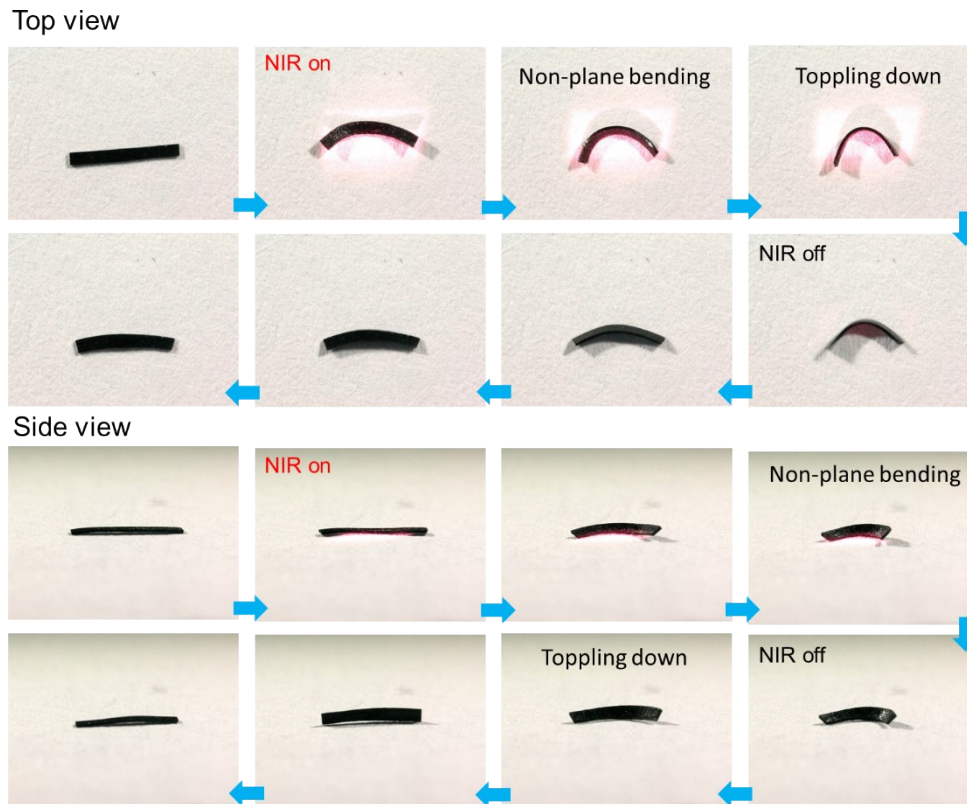
Figure S11. The top and side view about rolling gait. The lateral light induced millirobot forming unstable non-plane bending, and then toppling down upon switching on/off NIR light, completing lateral rolling behavior.
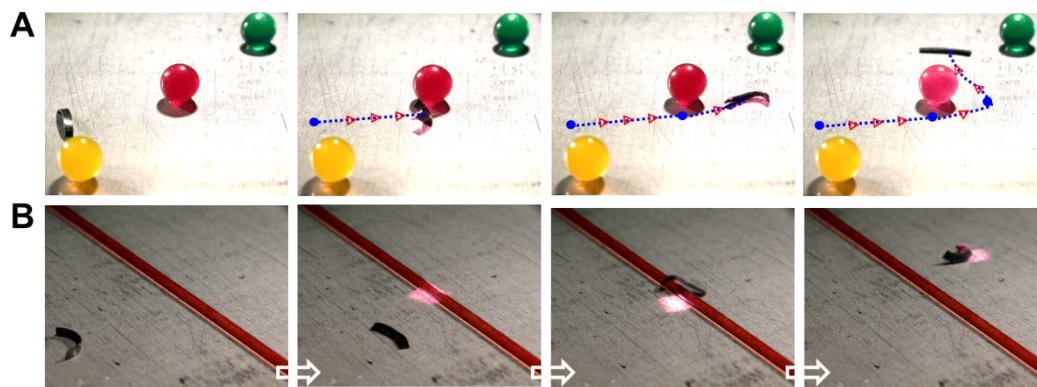
Figure S12. A) The digital pictures show the steering controllability traversing through obstacle course and "S" pathway depending on shifting locomotion behavior. B) The millirobot can cross through one hurdle with the aids of somersaulting locomotion behavior. The height of the hurdle is ∼0.71 mm.
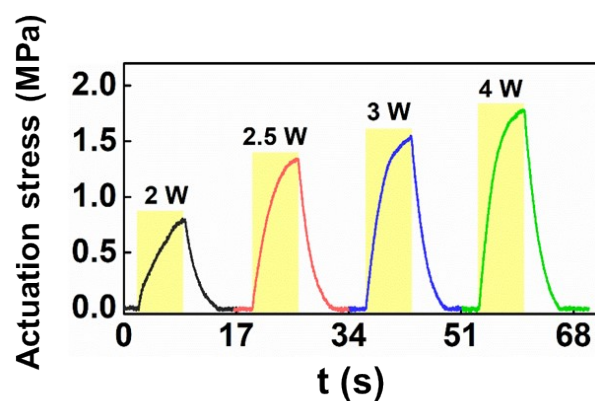
Figure S13. The actuation stress of millirobot at various NIR light intensity.

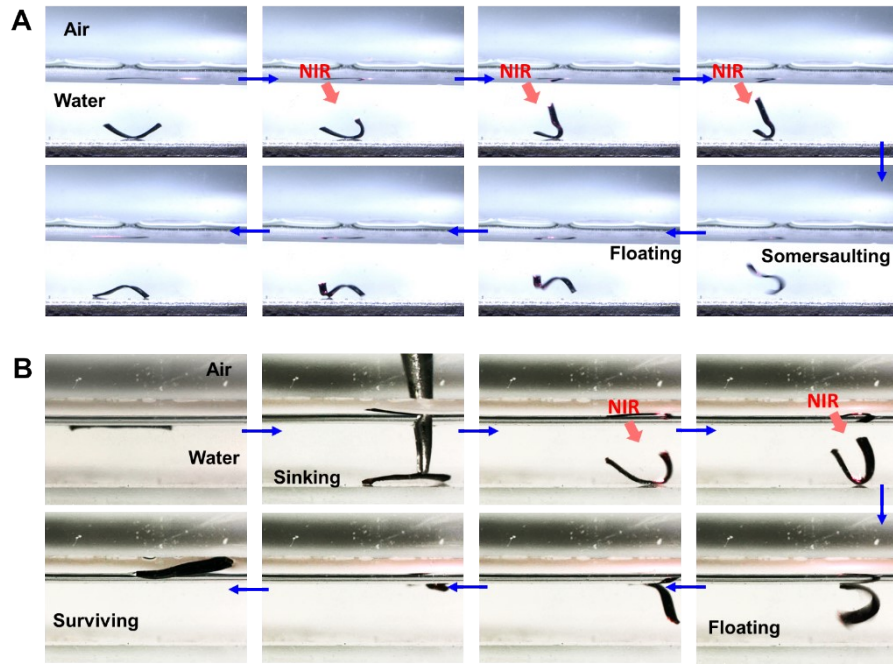**Figure S14.** Underwater locomotion performances. A) The millirobot performs larger shape morphing under NIR irradiation capable of somersaulting underwater. B) The millirobot is sunk by one tweezer and spontaneously float to water surface with the aids of NIR stimuli. The size of millirobot is about $5\lozenge0.5\lozenge0.12$ mm^3. Depth of water is 5 mm.

3. **Simulation**

Finite element package ABAQUS was employed to study the deformation mode of the LCE under illumination, in which the illumination was modeled as the temperature load. Specifically, thermal expansion was used to mimic the illumination induced mechanical deformation of the LCE. By fitting the experimental data of the deformation of the LCE under illumination, temperature-dependent thermal expansion was obtained and assigned to the LCEs. The mechanical properties of the LCE were described by the Fung-Orthotropic model, which was built-in material model in ABAQUS. Solid

element C3D8R was used in the simulation. We performed static analysis using Abaqus/Standard, in which the gravity field was applied in the direction perpendicular to the ground and the friction coefficient between LCE and ground was included.
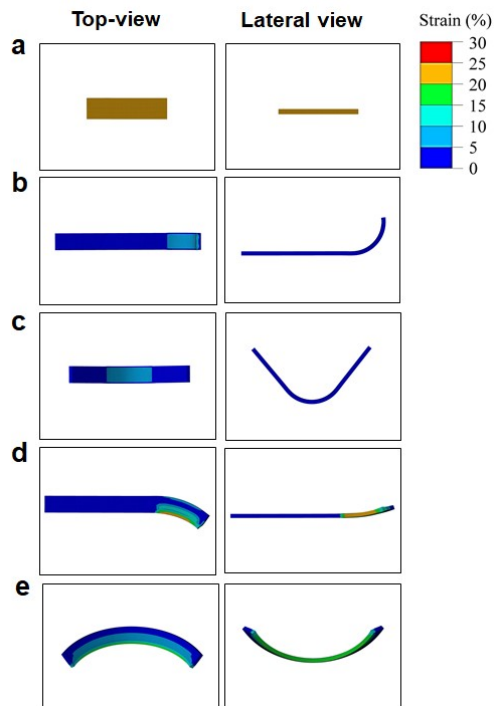
Figure S15. Simulation results showing uniform contraction (**a**), partially bending (**b**), V-shaped bending (**c**), non-plane J-shaped bending (**d**), and non-plane C-shaped bending (**e**), respectively.

Table S1. Summary of important performances of representative light-driven miniature soft robots reported over the last few years.

Ref	Materials	Deformation Mechanism	Locomotion modes
Angew. Chem. Int. Ed. 2013, 52, 9234	Single-wall carbon nanotube-liquid crystal elastomer composite/silicone bilayer film	Photo-thermal induced phase transition of liquid crystal elastomers	1. Crawling
Adv. Fun. Mater., 2014, 24, 7598.	Bilayer film composed of a pure PDMS layer and a PDMS/Graphene nanoplatelets composited layer	Different thermal expansion and Young's modulus of each layer	1. Swimming 2. Turning
Adv. Mater. 2015, 27, 3883	Azo-containing liquid crystal network	Photo-thermal induced phase transition of liquid crystal networks	1. Walking 2. Rotation 3. Jumping
Adv. Optical Mater. 2016, 4, 1689	Dye-doped liquid crystal network film	Photo-thermal induced phase transition of liquid crystal networks	1. Crawling 2. Squeezing
Nat. Mater. 2016, 15, 647	Azo-containing liquid crystal elastomer	Photo-thermal induced phase transition of liquid crystal elastomers	1. Swimming 2. Rotation
Angew. Chem. Int. Ed. 2018, 57, 11758	Dye-doped liquid crystal elastomer	Photo-thermal induced phase transition of liquid crystal elastomers	1. Crawling 2. Turning
Macromol. Rapid Commun. 2018, 39, 1700224	Dye-doped liquid crystal network film	Photo-thermal induced phase transition of liquid crystal networks	1. Crawling
Adv. Mater. Technol. 2019, 4, 1900185	Carbon-nanotube-doped liquid crystal elastomers film	Photo-thermal induced phase transition of the liquid crystal elastomers	1. Crawling 2. Jumping 3. Squeezing
Adv. Mater. 2020, 32, 1906233	Dye-doped liquid crystal network film	Photo-thermal induced phase transition of liquid crystal networks	1. Rolling
Our work	Photoactive LCEs using chemically bonded NIR groups	Photo-thermal induced phase transition of the liquid crystal elastomers	1. Crawling 2. Shifting 3. Rotation 4. Turning 5. Rolling 6. Somersaulting 7. Self-rocking 8. Swimming

References

[1] Liu, L., Liu, M. H., Deng, L. L., Lin, B. P., & Yang, H.. *J. Am. Chem. Soc.* **139**, 11333-11336 (2017).